


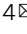




Cross-scale analysis of temperature compensation in the cyanobacterial circadian clock system

Yoshihiko Furuike^{1,2,8}, Dongyan Ouyang^{1,8}, Taiki Tominaga^{3,8} , Tatsuhiro Matsuo^{4,6,7} , Atsushi Mukaiyama^{1,2}, Yukinobu Kawakita⁵, Satoru Fujiwara⁴   & Shuji Akiyama^{1,2}  

Circadian clock proteins often reveal temperature-compensatory responses that counteract temperature influences to keep their enzymatic activities constant over a physiological range of temperature. This temperature-compensating ability at the reaction level is likely crucial for circadian clock systems, to which the clock proteins are incorporated, to achieve the system-level temperature compensation of the oscillation frequency. Nevertheless, temperature compensation is yet a puzzling phenomenon, since side chains that make up the clock proteins fluctuate more frequently due to greater thermal energy at higher temperature. Here, we investigated temperature influences on the dynamics of KaiC, a temperature-compensated enzyme (ATPase) that hydrolyzes ATP into ADP in the cyanobacterial circadian clock system, using quasielastic neutron scattering. The frequency of picosecond to subnanosecond incoherent local motions in KaiC was accelerated by a factor of only 1.2 by increasing the temperature by 10 °C. This temperature insensitivity of the local motions was not necessarily unique to KaiC, but confirmed also for a series of temperature-sensitive mutants of KaiC and proteins other than clock-related proteins. Rather, the dynamics associated with the temperature-compensatory nature of the reaction- and system-level was found in global diffusional motions, which was suggested to regulate the temperature dependence of ATPase activity and dephosphorylation process presumably through changes in the hexamer conformation of KaiC. The spatiotemporal scale at which cross-scale causality of the temperature sensitivity is established is finite, and extends down to picosecond to subnanosecond dynamics only in a very limited part of KaiC, not in its entire part.

¹Research Center of Integrative Molecular Systems, Institute for Molecular Science, National Institutes of Natural Sciences, 444-8585 Okazaki, Japan.

²Department of Functional Molecular Science, SOKENDAI (The Graduate University for Advanced Studies), 444-8585 Okazaki, Japan. ³Neutron Science and Technology Center, Comprehensive Research Organization for Science and Society (CROSS), 162-1 Shirakata, Tokai, Ibaraki 319-1106, Japan. ⁴Institute for Quantum Life Science, National Institutes for Quantum Science and Technology, 2-4 Shirakata, Tokai, Ibaraki 319-1106, Japan. ⁵J-PARC center, Japan Atomic Energy Agency, 2-4 Shirakata, Tokai, Ibaraki 319-1195, Japan. ⁶Present address: Laboratoire Interdisciplinaire de Physique (LiPhy), Grenoble-Alpes University, 140 rue de la physique, 38402 Saint Martin d'Hères, France. ⁷Present address: Institut Laue-Langevin, 71 avenue des Martyrs, CS 20156, 38042 Grenoble Cedex 9, France. ⁸These authors contributed equally: Yoshihiko Furuike, Dongyan Ouyang, Taiki Tominaga. ✉email: fujiwara.satoru@qst.go.jp; akiyamas@ims.ac.jp

Circadian clocks are endogenous timing systems that rhythmically control various biological processes with an ~24-h period¹. This rhythm persists stably even without any external cues, and the period length is kept constant even when ambient temperature changes (temperature compensation). The phase of the clock system can be shifted upon receiving external stimuli such as light and temperature and then synchronized to the phase of the outer world. These unique characteristics enable organisms to optimize their fitness during day/night environmental cycles^{2–5}.

Temperature compensation is a remarkable characteristic of the circadian clock systems. Q10 values, the factor by which reaction speed or cycle frequency is accelerated by increasing the ambient temperature by 10 °C, are mostly in the range of 0.9–1.1 for circadian clock systems, whereas those of most biochemical reactions⁶ and the Belousov–Zhabotinsky oscillator^{7–10} range from 2 to 3. As schematically shown in Fig. 1a, circadian clocks exhibiting system-level temperature compensation often comprise unique clock proteins with temperature-compensated biochemical

activities such as adenosine triphosphate (ATP) hydrolysis (ATPase)^{11–13}, and protein phosphorylation (kinase)^{14–16} and dephosphorylation (phosphatase)^{14,15}. A simple but attractive idea that emerged from studies^{12,13,15,17,18} of these biochemical activities is that the reaction-level temperature compensability is somehow correlated to system- or even higher cell-level temperature compensability (Fig. 1a). A great deal of effort has been devoted to elucidating the mechanism of this connectivity via experimental^{12,13,15,16,18} and modeling^{19–23} approaches.

Nevertheless, temperature compensation remains a puzzling phenomenon in terms of protein dynamics, as atoms and side chains in proteins should fluctuate more frequently at higher temperature due to their greater thermal energy. Three extreme cases can be considered (inset in Fig. 1a). First, thermal fluctuation in these key clock proteins is accelerated in a temperature-dependent manner, as observed for ordinary proteins. Second, the atoms and side chains in temperature-compensated clock proteins fluctuate in a temperature-insensitive manner via unknown mechanisms. Third, some opposing but balancing contributions

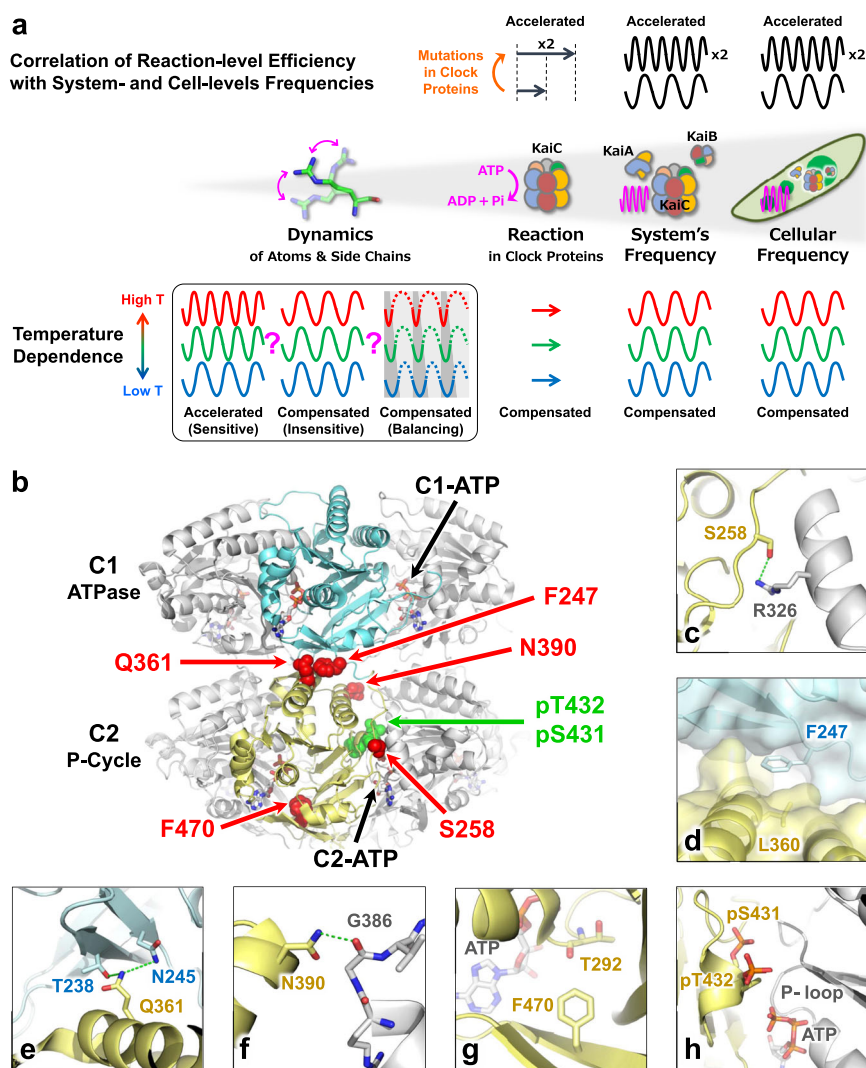


Fig. 1 Potential cross-scale causal relationship in the circadian clock system of cyanobacteria. **a** Spatiotemporal hierarchy spanning from atomic-scale dynamics, molecular-scale reaction, molecular system-scale frequency, and cellular-scale frequency. When the ATPase activity of KaiC doubles as a result of amino acid substitutions (orange arrow), both the in vitro system- and cell-level frequencies also double^{12,17,25}. In cyanobacteria, the temperature (T) sensitivity of ATPase is correlated with those of the system and cell levels. (Inset) Three extreme cases of temperature influence on clock-protein dynamics. Thermal fluctuations are sensitively accelerated, insensitively compensated, or sensitively compensated through a balance of opposing contributions. **b** Temperature-dependent ATPase mutation sites mapped onto the crystal structure of KaiC^{32,33}. Zoomed-in-views of **c** S258, **d** F247, **e** Q361, **f** N390, **g** F470, and **h** phosphorylated S431 and T432 in KaiC. Hydrogen bonds are highlighted by green dotted lines.

act at the level of protein dynamics level, i.e., one contribution accelerates but the other decelerates so that they differentially affect the elementary reaction steps to achieve overall compensation. Experimental investigations of the dynamics of temperature-compensated clock proteins are needed to distinguish among these cases.

KaiC, a temperature-compensated clock protein in cyanobacterium *Synechococcus elongatus* PCC 7942^{11–13}, acts as a circadian oscillator with other two clock proteins, KaiA and KaiB²⁴. Its most striking feature is that its temperature-compensated circadian rhythm can be reconstructed even in vitro by mixing KaiA, KaiB, and KaiC in the presence of ATP²⁵ (Fig. 1a). An ATP molecule binds a Walker motif in each of the tandemly duplicated domains called the N-terminal C1 and C-terminal C2 domains (Fig. 1b). These ATP binding events trigger oligomerization of KaiC into a double-ring hexamer. The ATP molecule bound to the C2 domain (C2-ATP) is used mostly as the source of phosphoryl group that is transferred to (auto-kinase) and then removed from (auto-phosphatase) S431 and T432 in KaiC. In the presence of KaiA and KaiB, the status of the dual phosphorylation site alters in a cyclic manner: ST → SpT → pSpT → pST → ST, where S, T, pS, and pT represent S431, T432, phosphorylated S431, and phosphorylated T432, respectively^{26,27}. The frequency of this phosphorylation cycle (P-cycle) is proportional to the rate of hydrolysis of C1-bound ATP (C1-ATP) into adenosine diphosphate (ADP) in the absence of KaiA and KaiB (Fig. 1a)^{12,13,17}. More importantly, the ATPase activity of KaiC is perfectly temperature-compensated ($Q_{10_{\text{ATP}}} = 1.0$)¹². The in vitro Kai oscillator that consists of temperature-compensated KaiC provides a practical means for studying cross-scale properties of temperature-compensation phenomena at the system, reaction, and dynamics levels (Fig. 1a).

Quasielastic neutron scattering (QENS) is a powerful and direct technique for accessing protein dynamics at the picosecond to nanosecond time scales²⁸. Because hydrogen atoms, which constitute up to half of all atoms in proteins, are distributed near uniformly in the three-dimensional structures of proteins, an averaged view of protein dynamics can be extracted from QENS spectra²⁹. In this study, we designed a series of KaiC mutants (Fig. 1b) with temperature-dependent periods (Fig. 1c–e), inverse temperature-dependent period (Fig. 1f), temperature-compensated but shortened-period (Fig. 1g), or arrhythmicity (Fig. 1h), and measured the temperature sensitivity of their protein dynamics using the neutron spectrometer BL02 (DNA: Biomolecular Dynamics Spectrometer) in the Material and Life Science Experimental Facility of Japan Proton Accelerator Research Complex (MLF/J-PARC)³⁰. Our QENS data revealed that the frequency of picosecond to sub-nanosecond incoherent motions is essentially temperature-insensitive in KaiC, regardless of the presence or absence of the temperature-sensitive mutations. The spatiotemporal scale at which cross-scale causality of the temperature sensitivity is established is finite, and extends down to picosecond to sub-nanosecond dynamics only in a very limited part of KaiC, not in its entire part.

Results

Screening and characterization of temperature-sensitive mutants of KaiC. As confirmed by the positions along the horizontal axis in Fig. 2a, the ATPase activity of KaiC^{WT} is as low as 11 d⁻¹ and almost temperature-insensitive ($Q_{10_{\text{ATP}}}^{\text{WT}} = 0.89 \pm 0.10$), as previously reported¹². Consistently with previous studies^{11,15,25}, the P-cycle frequency ($f_p = 24/\text{period}$) of KaiC^{WT} in the presence of KaiA and KaiB was also temperature-compensated (Fig. 2b) ($Q_{10_{f_p}}^{\text{WT}} = 1.08 \pm 0.04$). Consequently, data points taken at different temperatures for KaiC^{WT} nearly

overlapped in the ATPase- f_p plot (Fig. 2a). Taking advantage of potential reaction–system correlations, we screened the temperature-sensitive mutants of KaiC using an in vitro ATPase-based screening system³¹. Among a number of KaiC mutants screened for temperature-dependent ATPase activity, four candidates were characterized in detail as they revealed stable but temperature-dependent system-level oscillation (Fig. 2c–f).

The first was the S258A mutant of KaiC (KaiC^{S258A}). According to the X-ray crystal structure of KaiC^{WT}^{32,33}, S258 is located in the C2 domain (Fig. 1b and c). The ATPase activity of KaiC^{S258A} at 303 K ($6.3 \pm 1.1 \text{ d}^{-1}$) was lower than that of KaiC^{WT} ($11.8 \pm 1.1 \text{ d}^{-1}$) but increased in a temperature-dependent manner up to $14.1 \pm 1.8 \text{ d}^{-1}$ at 318 K ($Q_{10_{\text{ATP}}}^{\text{S258A}} = 1.73 \pm 0.22$) (Fig. 2a). Consistent with this, the f_p value for KaiC^{S258A} increased from 0.78 to 1.40 d^{-1} as the temperature increased (Fig. 2c) ($Q_{10_{f_p}}^{\text{S258A}} = 1.56 \pm 0.01$). Because of this correlation, the data trace for KaiC^{S258A} extends almost diagonally from low- to high-temperature conditions in the ATPase- f_p plot (Fig. 2a). The second and third mutants (KaiC^{F247A}, KaiC^{Q361E}), which replaced residues that neighbored in the C1–C2 interface (Figs. 1b, 2d, and e), are also traced diagonally (Fig. 2a). The f_p value for KaiC^{F247A} increased from 1.12 to 1.97 d^{-1} as temperature increased (Fig. 2d) ($Q_{10_{f_p}}^{\text{F247A}} = 1.63 \pm 0.01$), as observed for the mutant's ATPase activity (Fig. 2a) ($Q_{10_{\text{ATP}}}^{\text{F247A}} = 1.47 \pm 0.05$), whereas KaiC^{Q361E} exhibited a slightly weakened correlation between $Q_{10_{\text{ATP}}}^{\text{Q361E}}$ (1.70 ± 0.15) and $Q_{10_{f_p}}^{\text{Q361E}}$ (1.23 ± 0.02) (Fig. 2e and h). The fourth is an inverse temperature-dependent mutant that harbors the N390A substitution in the C2–C2 interface (KaiC^{N390A}, Fig. 1f) nearby the C1 domain (Fig. 1b). The ATPase activity and f_p value of KaiC^{N390A} became smaller at higher temperatures (Fig. 2f) in a correlated manner, as evidenced by its diagonal trace (Fig. 2a) with inverted temperature sensitivities ($Q_{10_{\text{ATP}}}^{\text{N390A}} = 0.47 \pm 0.07$, $Q_{10_{f_p}}^{\text{N390A}} = 0.69 \pm 0.02$). However, KaiC^{N390A} became arrhythmic at the highest temperature of 318 K (Fig. 2f).

Taking into consideration the limited persistence of the P-cycle for KaiC^{F247A} and KaiC^{N390A} at 318 K (Fig. 2d and f), we dissolved KaiC^{WT} and the four KaiC mutants exhibiting reaction–system correlation in a D₂O buffer (Supplementary Note 1) and subjected them to QENS experiments at different temperatures: 283, 293, 302, 313, and 317 K for KaiC^{WT}, 302 (low) and 310 or 313 K (high) for KaiC^{S258A}, KaiC^{F247A}, KaiC^{Q361E}, and KaiC^{N390A}. For comparison purposes, we conducted further QENS experiments using two other KaiC mutants^{12,25}; a temperature-compensated but period-shortened F470Y mutant of KaiC (KaiC^{F470Y}; $Q_{10_{\text{ATP}}}^{\text{F470Y}} = 1.07 \pm 0.06$ and $Q_{10_{f_p}}^{\text{F470Y}} = 1.09 \pm 0.05$) (Figs. 1b, 1g, 2a, 2g, and 2h) and a temperature-compensated but arrhythmic S431D/T432E double mutant (KaiC^{DE}; $Q_{10_{\text{ATP}}}^{\text{DE}} = 0.98 \pm 0.07$) mimicking the fully phosphorylated KaiC-pSpT (Figs. 1b, 1h, 2a, and 2h). Noted that the circadian rhythm of KaiC^{WT} was barely influenced by the D₂O buffer used in this study (light blue circles in Fig. 2b).

KaiC dynamics detected by QENS. To investigate the temperature dependence of KaiC dynamics, we conducted QENS experiments of KaiC^{WT} at five different temperatures from 283 to 317 K. It must be noted that 293 K is approximately the critical temperature of the in vitro oscillator³⁴, below which the P-cycle becomes arrhythmic (zero amplitude). As shown in Fig. 3a, a difference QENS spectrum $S(Q, E)$ of KaiC^{WT}, where Q is the momentum transfer and E is the energy transfer of neutrons, could be obtained at each temperature by subtracting the background spectrum of the D₂O solvent from the sample spectrum, on the basis of scaling factors calculated from neutron scattering cross-sections. The resultant $S(Q, E)$ for KaiC^{WT} at all the

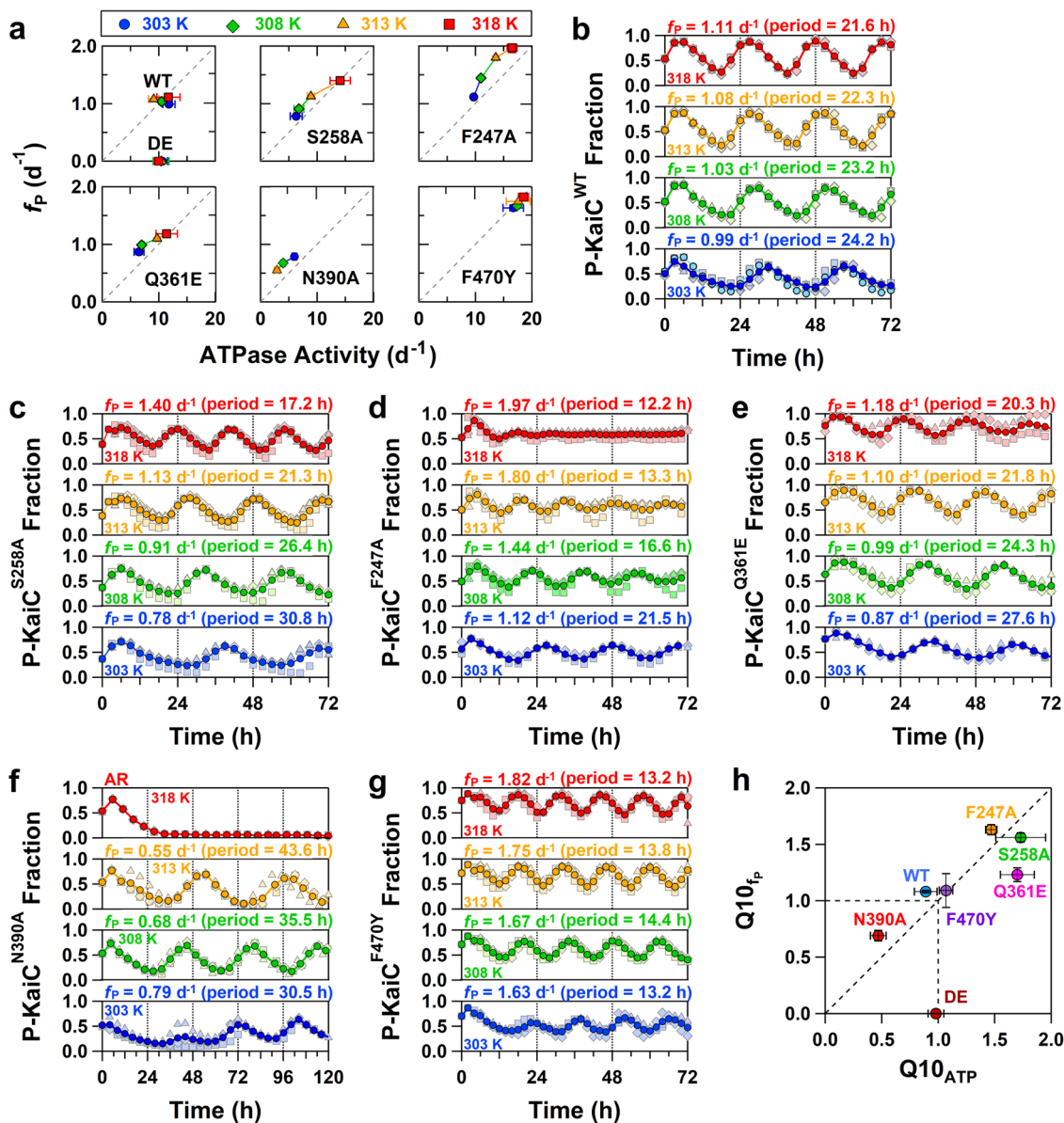


Fig. 2 Screening and characterization of temperature-sensitive mutants of KaiC. **a** Temperature dependence of the relationship between the ATPase activity of KaiC alone and in vitro KaiC phosphorylation-cycle (P-cycle) frequency ($f_p = 24/\text{period}$) in the presence of KaiA and KaiB. P-cycles of **b** KaiC^{WT}, **c** KaiC^{S258A}, **d** KaiC^{F247A}, **e** KaiC^{Q361E}, **f** KaiC^{N390A}, **g** KaiC^{F470Y} at four different temperatures: 303 (blue), 308 (green), 313 (orange), and 318 K (red). Dark-colored circles correspond to the mean from independent preparations and measurements (pale-colored squares, triangles, and diamonds). Light blue circles plotted in panel **b** correspond to the P-cycle of KaiC^{WT} in a D₂O buffer. **h** Correlation of Q_{10} values between ATPase ($Q_{10,ATP}$) and P-cycle ($Q_{10,P}$). Error bars correspond to one standard deviation obtained from three independent experiments, except that they are shown as three standard deviations for $Q_{10,P}$.

temperatures shared a common feature of temperature-dependent broadening of a narrow elastic peak and a wide quasi-elastic component derived from global and local motions, respectively (Fig. 3a). To analyze the Q- and temperature dependencies of these two components quantitatively, we attempted to fit the following equation²⁸ to each $S(Q,E)$ in Fig. 3b–f:

$$S(Q, E) = [A_0(Q)\delta(E) + \{1 - A_0(Q)\}L_{\text{local}}(Q, E)] \times L_{\text{global}}(Q, E) \times RF(Q, E) + BG(Q) \quad (1)$$

where $A_0(Q)$ is the elastic incoherent structure factor (EISF); $\delta(E)$ is Dirac delta function; $RF(Q,E)$ is the instrumental resolution function obtained from the spectrum of vanadium; $BG(Q)$ is the

background; and $L_{\text{local}}(Q,E)$ and $L_{\text{global}}(Q,E)$ are Lorentzian functions, $(\Gamma(Q)/\pi) (E^2 + \Gamma(Q)^2)^{-1}$, describing local internal motion and global diffusive motion of the protein, respectively, where $\Gamma(Q)$ is the half-width at half maximum. Q-averaged χ^2 values resulting from fitting of Eq. (1) to the experimental data of KaiC^{WT} was $\sim 0.93 \pm 0.07$ (Fig. 3b–f), assuring optimum quality of the curve-fitting procedure.

For the KaiC mutants, QENS experiments were conducted at low (302 K) and high (310 or 313 K) temperatures that were within the physiologically functional range of temperature as the circadian clock. Although most of the KaiC mutants showed similar $S(Q,E)$ to KaiC^{WT} (Fig. 4a, 4c, 4e, and 4f), visually distinguishable differences were observed for KaiC^{F247A} and KaiC^{N390A} (Fig. 4b and d). In order to make more detailed and quantitative comparisons, each $S(Q,E)$ of the KaiC mutants was

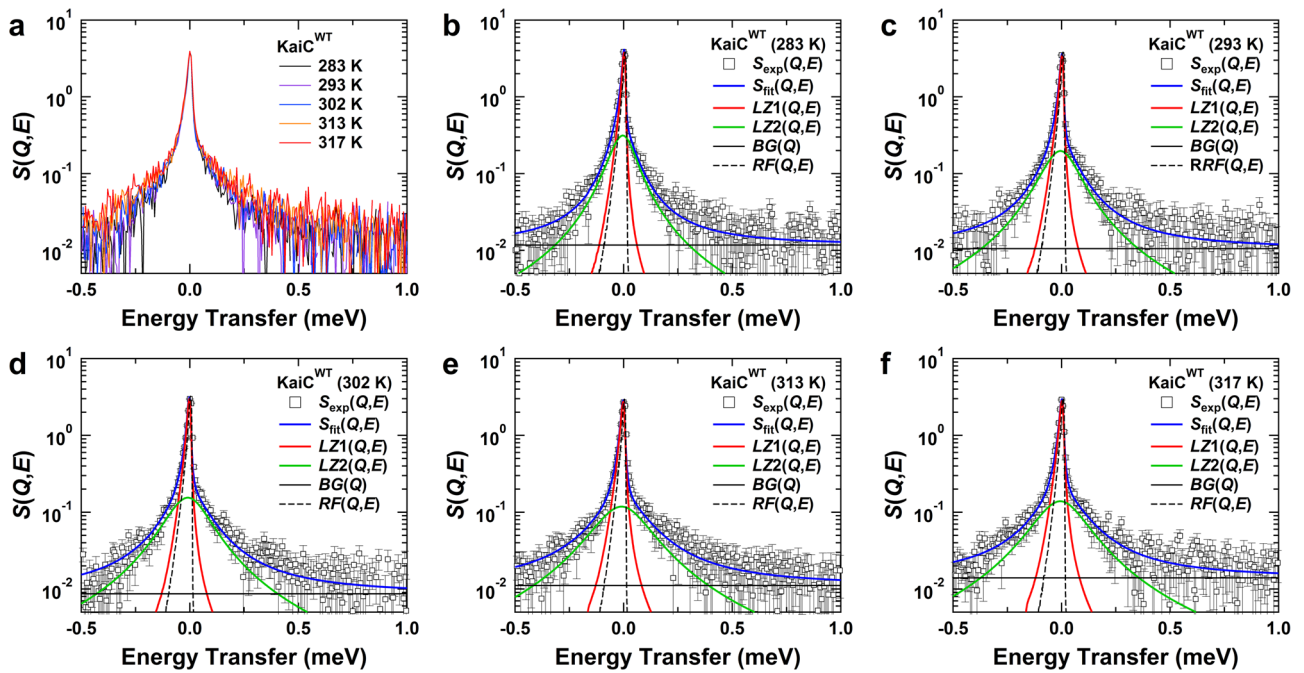


Fig. 3 Representative quasielastic neutron scattering (QENS) spectra, $S(Q,E)$, of KaiC^{WT} at $Q = 1.05 \text{ \AA}^{-1}$. **a** $S(Q,E)$ measured at five different temperatures from 283 to 317 K. Experimental spectra, $S_{\text{exp}}(Q,E)$, at **b** 283 K, **c** 293 K, **d** 302 K, **e** 313 K, and **f** 317 K are fitted using $S_{\text{fit}}(Q,E)$, which includes contributions of two Lorentzian functions, $LZ1(Q,E) = L_{\text{global}}(Q,E)$ and $LZ2(Q,E) = L_{\text{global}}(Q,E) \times L_{\text{local}}(Q,E)$, background $BG(Q)$, and resolution function $RF(Q,E)$ as defined in Eq. (1). The error bars come from the propagation of the standard deviation of the Poisson distribution in creating Q - E maps.

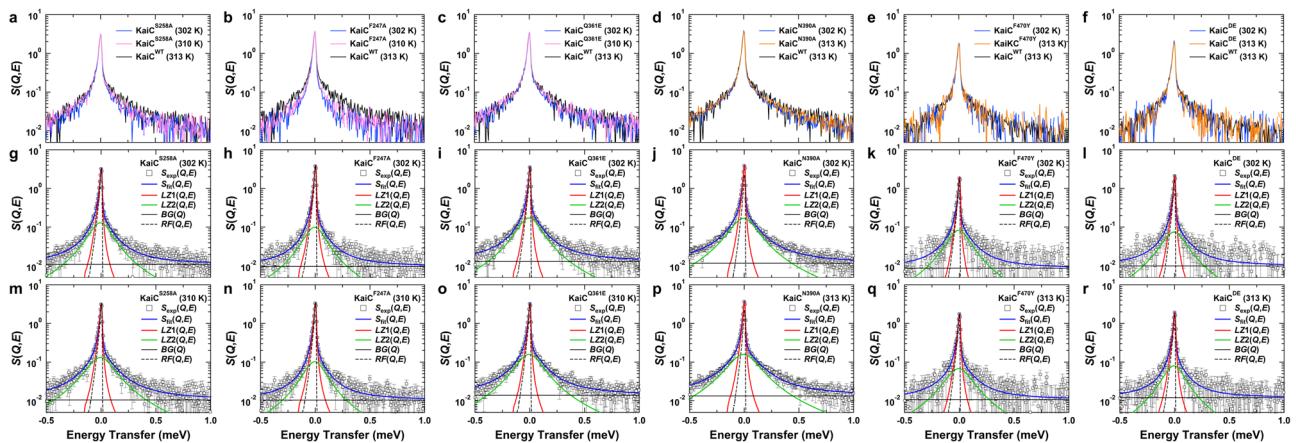


Fig. 4 Representative quasielastic neutron scattering (QENS) spectra, $S(Q,E)$, of KaiC mutants at $Q = 1.05 \text{ \AA}^{-1}$. Comparison of QENS spectra acquired at low and high temperatures for **a** KaiC^{S258A}, **b** KaiC^{F247A}, **c** KaiC^{Q361E}, **d** KaiC^{N390A}, **e** KaiC^{F470Y}, and **f** KaiC^{DE}. Blue, orange, and pink lines correspond to the spectra at 302, 313, and 310 K, respectively. For comparison, the QENS spectra of KaiC^{WT} at 313 K (black thick line) are normalized to match the top-peak intensity of the mutants. **g-l** At the low temperature of 302 K. **m-r** At a high temperature of 310 or 313 K. Experimental spectra, $S_{\text{exp}}(Q,E)$, are fitted using $S_{\text{fit}}(Q,E)$, which includes contributions of two Lorentzian functions, $LZ1(Q,E) = L_{\text{global}}(Q,E)$ and $LZ2(Q,E) = L_{\text{global}}(Q,E) \times L_{\text{local}}(Q,E)$, background $BG(Q)$, and resolution function $RF(Q,E)$ as defined in Eq. (1). The error bars come from the propagation of the standard deviation of the Poisson distribution in creating Q - E maps.

analyzed using Eq. (1) in the same way as KaiC^{WT} (panels g-r in Fig. 4). In the following, we describe the global and local motions of KaiC on the basis of temperature dependencies of $\Gamma_{\text{global}}(Q)$ and $\Gamma_{\text{local}}(Q)$, respectively.

Global motions of KaiC. $\Gamma_{\text{global}}(Q)$ provides information on the frequency of the global motions, whose properties are most straightforwardly inspected using the plot of $\Gamma_{\text{global}}(Q)$ vs Q^2 . Linear Q^2 -dependencies of $\Gamma_{\text{global}}(Q)$ were confirmed for KaiC^{WT} at every temperature (Fig. 5a), indicating its boundary-free diffusions including translational and rotational diffusions. Thus,

the linear slope in Fig. 5a relates to an apparent boundary-free diffusion coefficient (D_{global}). The D_{global} for KaiC^{WT} at 302 and 313 K were 3.54 ± 0.09 and $4.48 \pm 0.10 \times 10^{-7} \text{ cm}^2 \text{ s}^{-1}$, respectively (Fig. 5h), which were similar to those (3.75 and $4.97 \times 10^{-7} \text{ cm}^2 \text{ s}^{-1}$) calculated using the known crystal structure of the KaiC hexamer (Supplementary Note 2).

The temperature dependencies of the D_{global} ($Q10_{\text{global}}$) for KaiC^{WT} and the KaiC mutants (Fig. 5b-g) were ~ 1.2 (Fig. 5h), similar to other examples: ~ 1.2 (300–310 K) in human hemoglobin (Hb)³⁵ and ~ 1.2 (290–300 K) in α -synuclein (α Syn)³⁶. These observations are essentially consistent with the Stokes-Einstein diffusion that predicts $D_{\text{global}} \propto T/\eta(T)$, where T and $\eta(T)$ are the

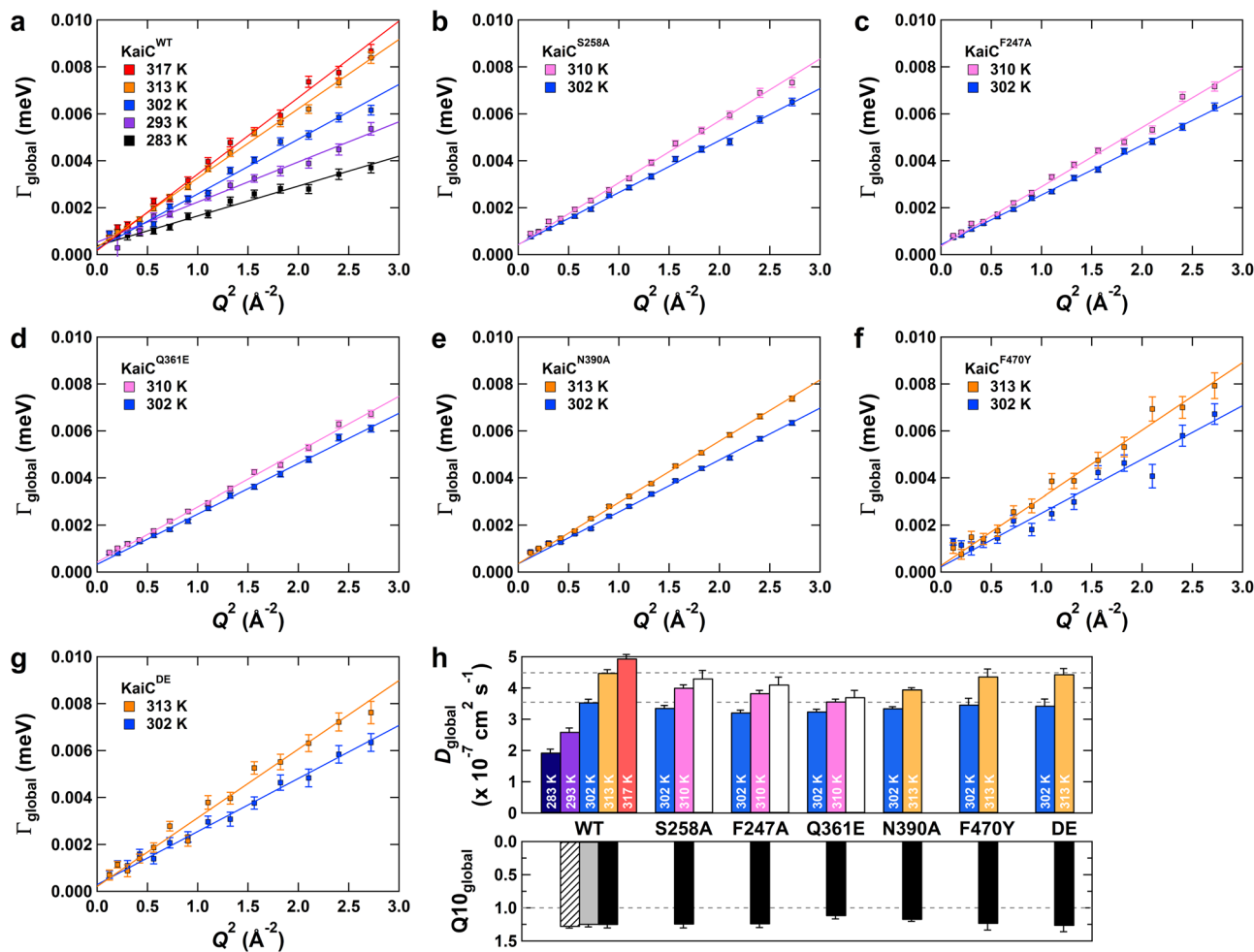


Fig. 5 Temperature- and Q^2 -dependences of global motions ($\Gamma_{\text{global}}(Q)$) in KaiC. **a** KaiC^{WT}, **b** KaiC^{S258A}, **c** KaiC^{F247A}, **d** KaiC^{Q361E}, **e** KaiC^{N390A}, **f** KaiC^{F470Y}, and **g** KaiC^{DE}. The slope of each linear fit corresponds to the apparent diffusion coefficient, D_{global} . Error bars correspond to the errors resulted from the curve-fitting analysis using Eq. (1) as shown in Figs. 3 and 4. **h** D_{global} and its temperature dependence, $Q_{10_{\text{global}}}$. White bars for KaiC^{S258A}, KaiC^{F247A}, and KaiC^{Q361E} correspond to the D_{global} values at 313 K, which were estimated by linear extrapolation of the D_{global} values determined at 302 and 310 K. A hatched bar represents $Q_{10_{\text{global}}}$ ^{WT} estimated from the slope of Arrhenius plot using five different temperatures (283, 293, 302, 313, and 317 K) (Supplementary Fig. 2a), as previously reported⁶⁵. A shaded bar represents $Q_{10_{\text{global}}}$ ^{WT} estimated from the slope of Arrhenius plot using three different temperatures (302, 313, and 317 K) within the physiologically functional range of temperature (Supplementary Fig. 2a). Other $Q_{10_{\text{global}}}$ presented as black bars were estimated as the ratio of measurement results (R_{Low} and R_{High}) at two temperatures (T_{Low} and T_{High}) using $Q_{10} = (R_{\text{High}}/R_{\text{Low}})^{10/(T_{\text{High}}-T_{\text{Low}})}$; $T_{\text{Low}} = 302 \text{ K}$, $T_{\text{High}} = 313$ or 310 K. Error bars correspond to the errors associated with the linear regression analysis (a-g).

temperature and solvent viscosity at T , respectively. Assuming $\eta(302) = 1.016 \text{ cP}$ and $\eta(313) = 0.799 \text{ cP}$ for the present D_2O solvent (Supplementary Note 2), the term of $T/\eta(T)$ increases 1.3-fold by raising the temperature from 302 to 313 K. This agreement between $Q_{10_{\text{global}}}$ and the increase ratio of $T/\eta(T)$ indicates that the temperature dependence of the hydrodynamic radius is rather small. Thus, we suggest that KaiC^{WT} and the KaiC mutants are maintained as intact hexamers during the QENS measurements in the observed temperature range.

In contrast to $Q_{10_{\text{global}}}$, the absolute D_{global} values of the temperature-sensitive mutants shared a common feature. The D_{global} values estimated at high temperature for KaiC^{S258A}, KaiC^{F247A}, KaiC^{Q361E}, and KaiC^{N390A} were systematically smaller than those of KaiC^{WT}, KaiC^{F470Y}, and KaiC^{DE} (Fig. 5h). In order to make a fair comparison, it is necessary to take into account that the measured temperature of KaiC^{S258A}, KaiC^{F247A}, KaiC^{Q361E} is lower by 3 K than the others. On the basis of the pseudo-linear temperature dependence of the D_{global} values for KaiC^{WT} (Fig. 5h), the D_{global} values at 313 K for KaiC^{S258A}, KaiC^{F247A}, KaiC^{Q361E} were estimated by linear extrapolation of the D_{global} values

determined at 302 and 310 K (white bars in Fig. 5h). Even after applying these corrections, the D_{global} values tended to be smaller in the temperature-sensitive mutants. These results suggest that the global hexamer structure of the temperature-sensitive mutants may be slightly different from those of KaiC^{WT} and the temperature-compensated KaiC mutants (KaiC^{F470Y}, KaiC^{DE}).

Local motions of KaiC. In contrast to $\Gamma_{\text{global}}(Q)$, $\Gamma_{\text{local}}(Q)$ reflects picosecond to sub-nanosecond incoherent local fluctuations of side-chain and main-chain in KaiC. $\Gamma_{\text{local}}(Q)$ of KaiC^{WT} increased asymptotically to approach a plateau at high Q^2 (Fig. 6a). As at high Q , the motions over short distances predominate, the plateau values correspond to the elementary displacements of the local motions. Slight but temperature-dependent increase in the high- Q plateau of KaiC^{WT} suggests that the side-chain and main-chain motions in KaiC^{WT} are accelerated by thermal fluctuations (Fig. 6a).

To determine the temperature sensitivity of the local motions quantitatively, Q^2 -dependencies of $\Gamma_{\text{local}}(Q)$ were analyzed by using a jump-diffusion model²⁸. $\Gamma_{\text{local}}(Q) = D_{\text{local}}Q^2$

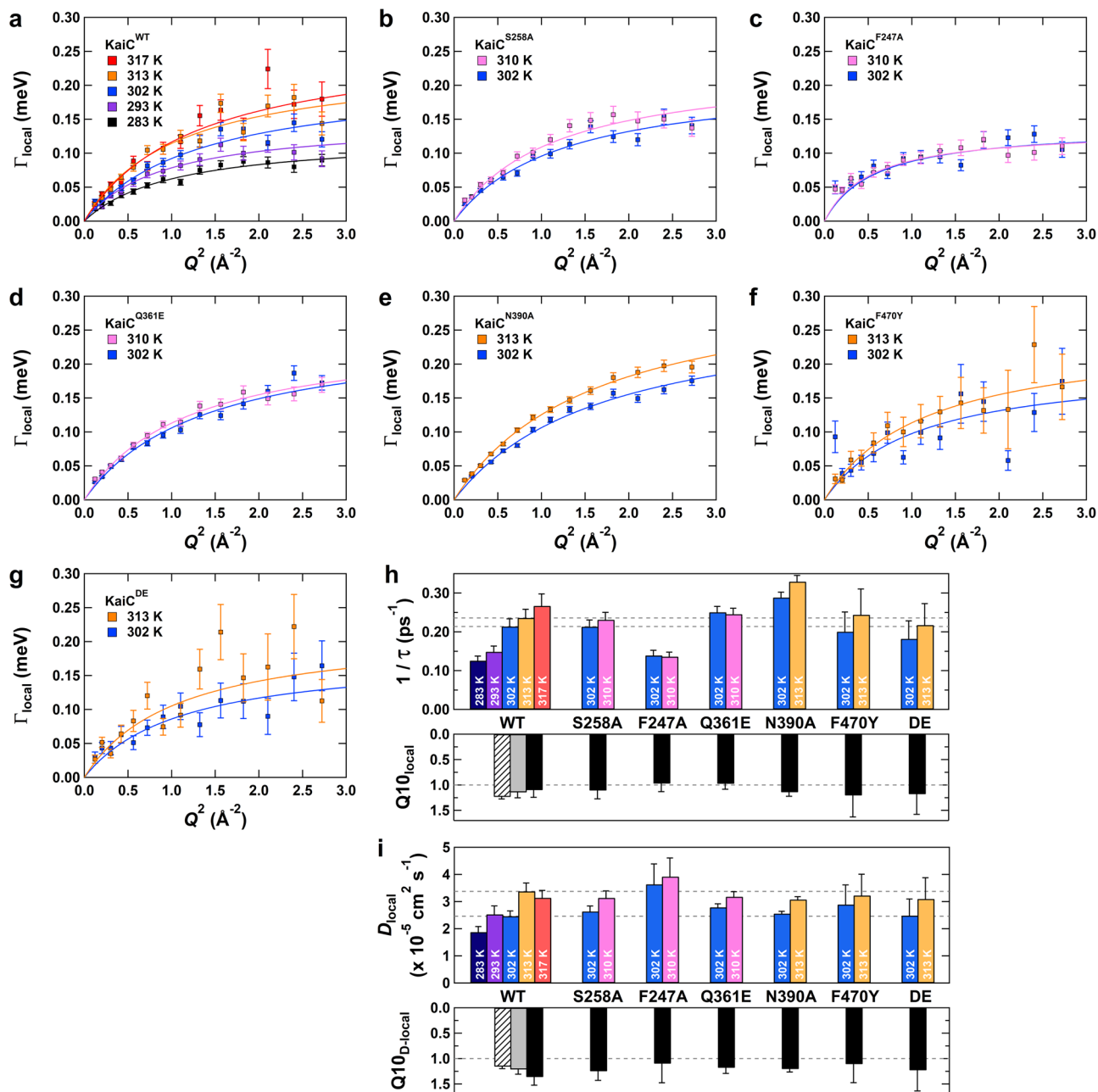


Fig. 6 Temperature- and Q^2 -dependences of local motions ($\Gamma_{\text{local}}(Q)$) in KaiC. **a** KaiC^{WT}, **b** KaiC^{S258A}, **c** KaiC^{F247A}, **d** KaiC^{Q361E}, **e** KaiC^{N390A}, **f** KaiC^{F470Y}, and **g** KaiC^{DE}. Solid lines represent resultant fits using a jump-diffusion model that predicts the jump-diffusion coefficient, D_{local} , as the curvature of the saturating curves and the reciprocal of residence time, τ^{-1} , as $\Gamma_{\text{local}}(Q)$ converged at infinite Q . Error bars correspond to the errors resulted from the curve-fitting analysis using Eq. (1) as shown in Figs. 3 and 4. **h** τ^{-1} and its temperature dependence, Q_{10}^{local} . **i** D_{local} and its temperature dependence, $Q_{10}^{\text{D-local}}$. A hatched bar represents $Q_{10}^{\text{local, WT}}$ or $Q_{10}^{\text{D-local, WT}}$ estimated from the slope of Arrhenius plot using five different temperatures (283, 293, 302, 313, and 317 K) (Supplementary Fig. 2b and 2c), as previously reported⁶⁵. A shaded bar represents $Q_{10}^{\text{local, WT}}$ or $Q_{10}^{\text{D-local, WT}}$ estimated from the slope of Arrhenius plot using three different temperatures (302, 313, and 317 K) within the physiologically functional range of temperature (Supplementary Fig. 2b and 2c). Other Q_{10}^{local} values presented as black bars were estimated as the ratio of measurement results (R_{Low} and R_{High}) at two temperatures (T_{Low} and T_{High}) using $Q_{10} = (R_{\text{High}}/R_{\text{Low}})^{10/(T_{\text{High}}-T_{\text{Low}})}$; $T_{\text{Low}} = 302 \text{ K}$, $T_{\text{High}} = 313$ or 310 K . Error bars correspond to the errors associated with the analysis using jump-diffusion model²⁸ (a-g).

$(1 + D_{\text{local}}Q^2\tau)^{-1}$, where D_{local} is the jump-diffusion coefficient and τ is the residence time spent on one site before jumping to others. The model gave reasonable fits to temperature- and Q^2 -dependent $\Gamma_{\text{local}}(Q)$ of KaiC^{WT} (lines in Fig. 6a). The resultant τ^{-1} values for KaiC^{WT} were slightly temperature-dependent (Fig. 6h). Arrhenius plot analyses using five different temperatures (283, 293, 302, 313, and 317 K) resulted in the activation energy of $4.0 \pm 0.6 \text{ kcal mol}^{-1}$ (Supplementary Note 3), which

corresponded to the Q_{10} value of 1.23 ± 0.04 for the internal motions (Q_{10}^{local} , hatched bar in Fig. 6h). The estimation of the $Q_{10}^{\text{local, WT}}$ value was not seriously affected by limiting the physiologically functional range of temperature (302, 313, and 317 K: $Q_{10}^{\text{local, WT}} = 1.15 \pm 0.11$, shaded bar in Fig. 6h, Supplementary Note 3) and by taking a ratio of τ^{-1} at low (302 K) and high (313 K) temperatures ($Q_{10}^{\text{local, WT}} = 1.10 \pm 0.14$, black bar in Fig. 6h). The Q_{10} values of D_{local} ($Q_{10}^{\text{D-local}}$) for KaiC^{WT} varied

in the range from 1.16 to 1.36 depending on the analysis method (Fig. 6i), probably due to the larger associated errors compared to the τ^{-1} values.

$\Gamma_{\text{local}}(Q)$ of the KaiC mutants, which revealed the same high- Q saturation as KaiC^{WT} (Fig. 6b–g), could be analyzed reasonably with the jump-diffusion model. Regardless of whether they are temperature-compensated or temperature-dependent, the $Q_{10_{\text{local}}}$ values of the KaiC mutants ranged from 0.97 to 1.20 and were comparable to KaiC^{WT} within error (Fig. 6h). A similar trend was confirmed for $Q_{10_{\text{D-local}}}$ (Fig. 6i). These results suggest that the average behavior of the local fluctuations occurring throughout KaiC, at least on picosecond to sub-nanosecond time scales, is not clearly correlated with the reaction and system levels in terms of temperature dependence.

While the mutations had small effects on the temperature dependence of the local dynamics, the absolute values of τ^{-1} were markedly different from KaiC^{WT} in several temperature-sensitive mutants. The τ^{-1} values for KaiC^{F247A} were $0.14 \pm 0.01 \text{ ps}^{-1}$ at low and high temperatures and were reduced ~50–70% relative to KaiC^{WT} (Fig. 6h). Conversely, the local motions in KaiC^{N390A} were 30–40% faster (0.29 ± 0.01 – $0.33 \pm 0.02 \text{ ps}^{-1}$) than KaiC^{WT} (Fig. 6h). D_{local} was essentially unaffected by temperature change or mutations (Fig. 6i), except in the case of KaiC^{F247A}, where a large error prevented us from identifying clear increase in D_{local} .

Fractional change in apparently immobile atoms in the temperature-dependent ATPase mutants of KaiC. EISF is defined as the ratio of the elastic peak intensity to the sum of elastic and quasielastic scattering intensities as in Eq. (1), providing information on the geometry of molecular motions and the fraction of mobile and immobile atoms on the time scale (~55 ps) of the spectrometer. As shown in Fig. 7a–g, EISF of KaiC^{WT} and the mutants were plotted against Q and then fitted using the following equation, assuming diffusion in an ensemble of spheres whose radii (a) follow a lognormal distribution³⁷:

$$\text{EISF}(Q) = p + (1 - p) \int_0^{\infty} \frac{1}{s\sqrt{2\pi a}} e^{-\frac{(\ln(a/c))^2}{2s^2}} \left[\frac{3j_1(Qa)}{Qa} \right]^2 da \quad (2)$$

where p is the fraction of atoms whose motions are outside the current instrumental energy window and therefore appear immobile; $(1 - p)$ correspond to the fraction of atoms diffusing within the sphere ensemble; c is the median of the distribution; s is the variance in the natural logarithmic space; and j_1 denotes the spherical Bessel function of the first kind of order.

The results of EISF analysis support the current observations on the local dynamics. Consistent with the $Q_{10_{\text{local}}}$ ^{WT} value of 1.15 ± 0.11 , the immobile fraction of KaiC^{WT} was maintained at ~0.6 in the physiologically functional range of temperature (Fig. 7h). In KaiC^{F470Y} and KaiC^{DE}, the immobile fractions were nearly unaffected by temperature change or mutations within the experimental error. On the other hand, the immobile fraction of KaiC^{F247A} increased 25% as the temperature increased, despite its nearly temperature-compensated τ^{-1} value ($Q_{10_{\text{local}}}$ ^{F247A} = 0.97 ± 0.16). Interestingly, a reverse trend was confirmed in KaiC^{N390A}. At the same time, all the temperature-sensitive mutants of KaiC exhibited smaller immobile fractions than KaiC^{WT} at 302 K. This result that the temperature-dependent mutations shifted certain motions from immobile to mobile fractions (Fig. 7h) is directly or indirectly related to the systematic decrease in the D_{global} values (Fig. 5h).

In KaiC^{WT} and KaiC^{F470Y}, atoms diffusing within a radius of 3–6 Å (Fig. 7i) constituted a major mobile component. By contrast, the mobile fractions of the temperature-sensitive mutants and KaiC^{DE} were distributed mainly in reduced radii of 1–2 Å relative to KaiC^{WT}. Thus, KaiC^{S258A}, KaiC^{F247A},

KaiC^{Q361E}, and KaiC^{N390A} are the temperature-dependent ATPase mutants with the reductions in D_{global} (Fig. 5h), immobile fraction p (Fig. 7h), and amplitudes of local motions (Fig. 7i).

Discussion

Over the past decades, chronobiologists have sought a reasonable model that explains the three physiological properties of the circadian clock systems: self-sustained oscillation, temperature compensation, and synchronization^{2–4}. The circadian clock of cyanobacteria is an ideal experimental system for this purpose, as its physiological properties can be studied in relation to the physicochemical properties of clock-related components at the molecular and atomic scales.

Among the three Kai proteins, KaiC is the core of the cyanobacterial clock system. In the presence of both KaiA and KaiB, KaiC exhibits a phosphorylation rhythm (Fig. 2b) whose frequency (f_p) is correlated with the ATPase activity of KaiC alone (Fig. 2a). For example, when the ATPase activity of KaiC doubles as a result of amino acid substitutions, the frequencies of both the in vitro system-scale and the cellular-scale rhythms also double (Fig. 1a)^{12,17,25}.

This causal relationship, in which properties are transferred through upward causation from bottom to top in the spatio-temporal hierarchy, was also confirmed for temperature compensation from the reaction to the cellular scale (Fig. 1a). The ATPase activity of KaiC^{WT} is temperature-compensated; probably because of this, both the in vitro and in vivo rhythms¹³ are also temperature-independent. This phenomenological interpretation is further supported by the four examples of temperature-sensitive mutants of KaiC. In contrast to KaiC^{WT} ($Q_{10_{\text{ATP}}}$ ^{WT} = 0.89 ± 0.10), the f_p values for KaiC^{S258A} ($Q_{10_{\text{ATP}}}$ ^{S258A} = 1.73 ± 0.22), KaiC^{F247A} ($Q_{10_{\text{ATP}}}$ ^{F247A} = 1.47 ± 0.05), and KaiC^{Q361E} ($Q_{10_{\text{ATP}}}$ ^{Q361E} = 1.70 ± 0.15) increased in a temperature-dependent manner (Fig. 2c–e), and the f_p value for KaiC^{N390A} ($Q_{10_{\text{ATP}}}$ ^{N390A} = 0.47 ± 0.07) obeyed the inverse temperature dependence (Fig. 2f). The well correlated Q_{10} values between the ATPase activity and f_p values in the four mutants (Fig. 2h) clearly demonstrate that the reaction-to-system scale causal relationship arises from the temperature-compensated ATPase activity of KaiC.

In the present study, we utilized QENS technique to test how far down the microscopic spatiotemporal scale the causality of the temperature sensitivity can be established. The $Q_{10_{\text{global}}}$ values were estimated to be ~1.2 for KaiC^{WT} and the mutants (Fig. 5h), confirming that the global motions of KaiC are accelerated by the temperature dependence of $T/\eta(T)$ according to the Stokes-Einstein diffusion law. The limited temperature dependence was also observed for the parameters, such as τ^{-1} and D_{local} , which characterize the local dynamics of KaiC. Even though the P-cycle and ATPase activity were accelerated in a temperature-dependent manner ($Q_{10_{\text{ATP}}}$ and $Q_{10_{\text{fp}}}$ as high as 1.7) in the three mutants (KaiC^{S258A}, KaiC^{F247A}, KaiC^{Q361E}) and decelerated in the inverse temperature-dependent manner ($Q_{10_{\text{ATP}}}$ and $Q_{10_{\text{fp}}}$ as low as 0.5) in one mutant (KaiC^{N390A}) (Fig. 2h), the $Q_{10_{\text{local}}}$ and $Q_{10_{\text{D-local}}}$ values for all the four temperature-sensitive mutants monotonously resulted in 1.0–1.2 (Fig. 6h and i). The similar temperature dependence was also confirmed for the local dynamics of the temperature-compensated but short-period (KaiC^{F470Y}) and arrhythmic (KaiC^{DE}) mutants. Our current QENS observations indicate that the spatiotemporal scale at which causality of the temperature sensitivity is established is finite. Given that QENS detects the average image of the fluctuations of all the hydrogen atoms scattered in the protein molecule, we can conclude that causality is established down to the local dynamics only in a very limited part of KaiC (inset in Fig. 1a).

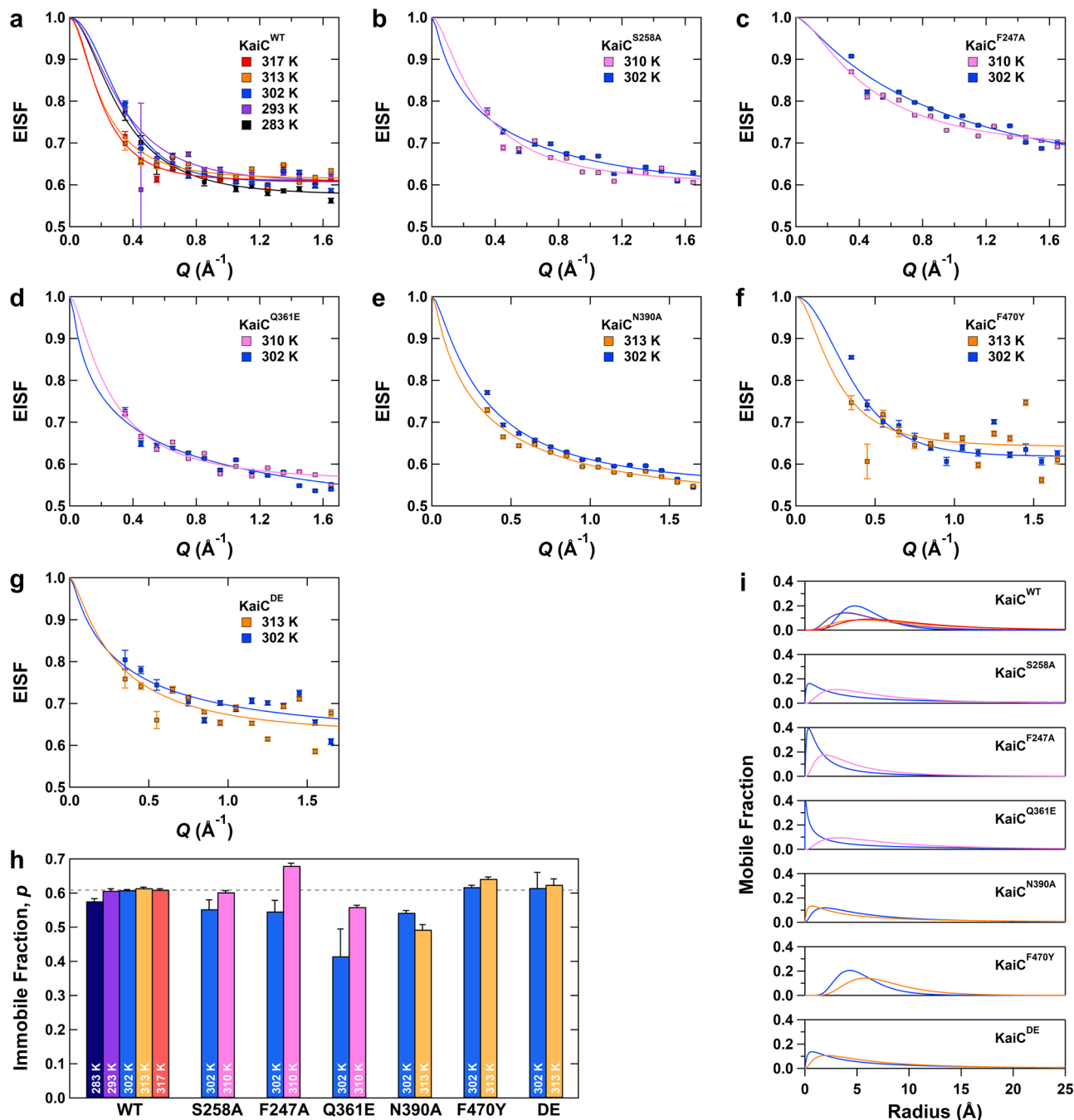


Fig. 7 Elastic incoherent structure factor (EISF) analyses under the assumption of sphere-ensemble model. **a** KaiC^{WT}, **b** KaiC^{S258A}, **c** KaiC^{F247A}, **d** KaiC^{Q361E}, **e** KaiC^{N390A}, **f** KaiC^{F470Y}, and **g** KaiC^{DE}. Solid lines represent the resultant fits of Eq. (2). Error bars correspond to the errors resulted from the curve-fitting analysis using Eq. (1) as shown in Figs. 3 and 4. **h** Immobile fraction, p . **i** Radial distribution functions of mobile fraction. Black, purple, blue, pink, orange, and red lines correspond to the distributions at 283, 293, 302, 310, 313, and 317 K, respectively. Error bars correspond to the errors associated with the EISF analysis³⁷ using Eq. (2) (a-g).

It is worth discussing our observations in the light of previous QENS studies on proteins other than clock-related proteins. To date, the QENS method has been used in many studies to characterize protein dynamics of small single-domain proteins^{38,39} to larger and more complex molecular systems^{40–43}, as well as to large-scale conformational changes such as those that occur upon ligand binding^{35,44,45}, pressurization^{46–48}, unfolding^{37,49–53}, and fibrillization^{36,54}. The results reported to date for various protein samples indicate that the τ values are mostly distributed in the range of 1–20 ps ($\tau^{-1} = 0.05\text{--}1.0\text{ ps}^{-1}$) (see Grimaldo et al.²⁹ and references therein), although attention must be paid to the differences in

measurement temperature, energy resolution, and analysis methods. The τ value for KaiC^{WT}, 3.7–8.0 ps ($\tau^{-1} = 0.13\text{--}0.27\text{ ps}^{-1}$), is included in the above range, indicating that the internal motion of KaiC^{WT} is neither exceptionally slow nor too fast.

More detailed comparisons of internal motions are possible by making reference for QENS data for Hb³⁵ and α Syn³⁶, which were acquired at the same beamline with the same energy resolution (12 $\mu\text{eV}/55\text{ ps}$). As shown in Fig. 8, the temperature dependence of the jump-diffusion frequency of KaiC^{WT} ($Q_{10,\text{local}}^{\text{WT}} = 1.1\text{--}1.2$) is not substantially different from the four examples ($Q_{10,\text{local}} = 1.1\text{--}1.3$) for deoxygenated Hb (deoxy-Hb),

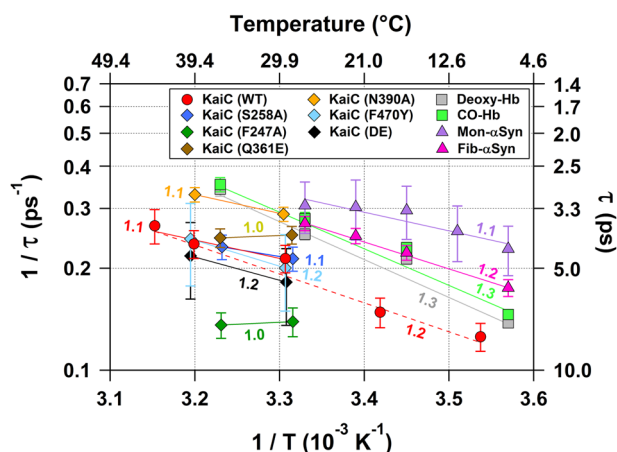


Fig. 8 Temperature dependences of jump-diffusion frequency (τ^{-1}) for KaiC, human hemoglobin (Hb), and α -synuclein (α Syn). Dashed and solid red lines represent the linear fits of the Arrhenius plot for KaiC^{WT} using entire (283–317 K) and physiologically functional range (302–317 K) of temperature, respectively. Quasielastic neutron scattering (QENS) data of Hb and α Syn are taken from previous studies^{35,36}; activation energies of deoxygenated Hb (deoxy-Hb), CO-bound Hb (CO-Hb), fibrillized α Syn (fib- α Syn), and monomeric α Syn (mon- α Syn) are 5.2 ± 0.3 , 5.2 ± 0.3 , 3.7 ± 0.7 , and 2.6 ± 1.9 kcal mol⁻¹, respectively. Values given near fitting lines represent the $Q_{10\text{local}}$ values estimated for 303 K.

CO-bound Hb (CO-Hb), a fibril state of α Syn (fib- α Syn), and a monomeric but intrinsically disordered form of α Syn (mon- α Syn). This result points to the intrinsically low energy barrier for the local motions independent of protein folds or functions, supporting the present interpretation that the temperature sensitivity of the Kai oscillator does not correlate well with that of the picosecond to sub-nanosecond local dynamics. In the measured range of temperature, however, the τ^{-1} values for KaiC^{WT} are 30–50% smaller than those of the four examples. Considering the insensitivity of the internal dynamics even upon an R(CO)-to-T(deoxy) allosteric transition of Hb (Fig. 8), we speculate that the slower jump-diffusion frequency of KaiC^{WT} may be related to its function and structure as the circadian pacemaker. In fact, the τ^{-1} values for KaiC^{F247A} and KaiC^{N390A} were 50–70% reduced and 30–40% enhanced, respectively, relative to KaiC^{WT} (Figs. 6h and 8), although not for all temperature-sensitive mutants.

In contrast to the featureless temperature dependence of the local motions, all the temperature-sensitive mutants shared the reduced global motions including the translational and rotational diffusions relative to KaiC^{WT} and temperature-insensitive mutants (KaiC^{F470Y} and KaiC^{DE}) (Fig. 5h). Two possibilities can be considered for the reduced D_{global} .

The first is the deformation into less compact hexamers by the temperature-sensitive mutations. According to the crystallographic structure of KaiC^{32,33}, every temperature-sensitive mutation is mapped onto its domain-domain interfaces. S258 is located in the outer radius side of the C2 ring (Fig. 1b); the side chain is hydrogen bonded to that of R326 in the neighboring C2 domain (Fig. 1c). This inter-C2-domain hydrogen bond is thus disrupted in KaiC^{S258A}. F247 and Q361 neighbor each other in the C1–C2 interface (Fig. 1b), which is stabilized by a limited number of inter-domain contacts with lower packing density than the C1–C1 and C2–C2 interfaces (Supplementary Note 4), exemplified by the non-bonded interactions associated with F247 and Q361 (Fig. 1b). The plane of the phenyl ring of F247 in the C1 domain lies nearly parallel to the C1–C2 interface (Fig. 1d), filling the loosely packed boundary through a hydrophobic interaction with L360 in the C2 domain. The F247A substitution is thus interpreted as the

mutation that makes the intrinsically low-density interface even looser. Although the C1–C2 packing density will be little affected by the replacement of glutamine to glutamate in KaiC^{Q361E} (Fig. 1b), a potential hydrogen bond between Q361 and either T238 or N245 in the C1 domain should be modulated or even disrupted (Fig. 1e). The N390A substitution disrupts the inter-C2-domain hydrogen bond between the side chain of N390 and the main-chain carbonyl oxygen atom of G386 (Fig. 1f). Considering these structural features common to the temperature-sensitive mutations, we speculate that the looser inter-domain interactions have resulted in the loss of compactness of the hexamer structure.

The second is the reduction of an additional contribution from internal large-scale motions. Previous QENS study on the R(CO)-to-T(deoxy) allosteric transition of Hb shows a certain similarity to our results³⁵; D_{global} is notably increased upon the T(deoxy)-to-R(CO) transition while keeping τ^{-1} nearly unaffected. Authors of that study suggested that internal large-scale relative motions of two $\alpha\beta$ dimers could partially contribute to D_{global} in CO-Hb³⁵. If this is the case, the decrease in D_{global} is interpreted as a result of the suppression of domains movements within the KaiC hexamer by the temperature-sensitive mutations. In fact, several lines of evidence have pointed out the dynamic properties of inter-ring stacking of KaiC during the circadian cycle⁵⁵.

Since the current temperature-sensitive mutations will not make the inter-domain interactions within the KaiC hexamer more stable, we believe that the contribution of the first case is greater than that of the second. This interpretation is also consistent with the decrease in the immobile fraction of the temperature-sensitive mutations (Fig. 7h). As shown in Fig. 2c–f, the temperature-sensitive mutations resulted in a preferential shortening and elongation of the dephosphorylation process in the P-cycle. The dephosphorylation process is also the timing of the ATPase activation in KaiC¹². Taken together, these results suggest that delicate but close inter-domain interactions are important in regulating the temperature dependence of ATPase and dephosphorylation reactions in KaiC. This view is also supported by the fact that the KaiC hexamer undergoes a quaternary structure change in concert with ATPase and dephosphorylation events³³.

Several studies have suggested that fluctuations and structural polymorphs of the clock proteins play important roles in the circadian clock systems. In mammalian systems, CKI δ -dependent phosphorylation is one of the key reactions that regulates period length and its temperature sensitivity¹⁶. In CKI δ , the temperature dependence of substrate affinity is compensated by the opposing temperature dependence of product affinity¹⁸. On the basis of molecular dynamics (MD) simulation, the authors of that study proposed that the temperature dependence of the amplitude of particular local fluctuations is reversed in the substrate- and product-bound forms, and that this reversal is one of the origins of the biochemical opposition. Structural polymorphs of the clock proteins, which have been confirmed by crystallography, NMR, and MD simulation, also play important roles in the substrate selectivity of CKI δ ⁵⁶ and the interaction between CRY1/2 and the CLOCK-BMAL1 complex⁵⁷. In the cyanobacterial system, the rhythmic stacking/unstacking of C1- and C2-rings is coupled to the P-cycle of KaiC⁵⁵. The MD simulation of ADP release from the C2 domain⁵⁸. These previous observations are mainly based on the MD simulations and experiments on nanosecond to microsecond time scales, which are much slower than the time scales targeted by the current QENS study.

The mechanism by which a single amino acid substitution can exert a notable effect on reaction- or even system-level temperature compensation deserves further investigation. There is growing experimental evidence that ordinary enzymes actively utilize internal motions, thereby increasing the efficiency of

overall catalytic reactions^{59–61}. Because functionally relevant fluctuations often refer to collective motions of atoms on slower time scales (μs to ms), care must be taken in discussing those motions in relation to the incoherent and fast (ps) dynamics detected in this study. However, several studies have demonstrated a linkage between ps–ns fluctuations and slower motions associated with catalytic reactions^{62–64}. Thus, it is necessary to experimentally verify the possibility that the causality of temperature sensitivity in KaiC is still established on limited time scales longer than nanoseconds.

Methods

Expression and purification of Kai proteins. Glutathione S-transferase (GST)-tagged versions of Kai proteins were constructed in pGEX-6P-1. Each Kai GST-fusion protein was expressed in *E. coli* BL21(DE3) and purified as reported previously^{11,26}.

ATPase assay. ATPase activities of KaiC^{WT} and its mutants, dissolved in an H₂O buffer (H1-buffer) including 20 mM Tris/HCl (pH 8.0), 150 mM NaCl, 5 mM MgCl₂, 1 mM DTT, 1 mM EDTA, and 1 mM ATP, were measured at 303, 308, 313, and 318 K as previously reported^{11,15}.

In vitro rhythm assay. P-cycles of KaiC^{WT} and its mutants (0.2 mg/ml) were initiated by addition of KaiA (0.04 mg/ml) and KaiB (0.04 mg/ml) in H1-buffer at 303, 308, 313, and 318 K²⁵. For KaiC^{F247A} and KaiC^{Q361E}, whose P-cycle were unstable or unobvious at the normal amount of KaiA, KaiA was added at a 2-fold higher concentration (0.08 mg/ml). Aliquots taken from the incubated samples were subjected to SDS-PAGE analysis. The relative abundances of four phosphorylation states of KaiC were quantified by densitometric image analysis of gel bands using the LOUPE software⁶⁵.

Sample preparation for QENS. Every sample was prepared on site immediately before QENS measurements. KaiC^{WT} and its mutants were purified on a gel-filtration column (Superdex 200 15/30, Cytiva) equilibrated with an H₂O buffer (H2-buffer) containing 50 mM Tris/HCl (pH 8.0), 150 mM NaCl, 5 mM MgCl₂, 3 mM DTT, 1 mM EDTA, and 20 mM ATP. Collected fractions were subjected to rapid buffer exchange in a D₂O buffer (D2-buffer) containing 50 mM Tris/HCl (pD 7.6), 150 mM NaCl, 5 mM MgCl₂, 3 mM DTT, 1 mM EDTA, and 20 mM ATP using a desalting column (HiPrep 50, Cytiva). KaiC^{WT}, KaiC^{S258A}, KaiC^{F247A}, KaiC^{Q361E}, KaiC^{N390A}, KaiC^{F470Y}, and KaiC^{DE} were concentrated up to 15.0, 12.3, 14.6, 14.3, 16.9, 8.5, and 9.7 mg/mL, respectively. Each 1-mL sample was placed in a double-cylindrical aluminum cell with a sample thickness of 0.5 mm and sealed tightly with indium wire.

QENS experiments. QENS data were recorded using the near-backscattering spectrometer installed at beamline BL02 (DNA) in the Material and Life Science Experimental Facility of Japan Proton Accelerator Research Complex (MLF/J-PARC), Tokai, Ibaraki, Japan³⁰. QENS spectra were recorded over an energy transfer range from -0.5 to 1.5 meV with energy resolution (12 μeV) enabling us to access motions faster than ~ 55 ps. QENS data were collected at 283, 293, 302, 310, 313, and 317 K with exposure times of 6–10 h for each condition (520–615 kW). The obtained $S(Q,E)$ were corrected for detector efficiency using a vanadium standard, and intensities were normalized as relative intensities using the standard after subtracting the contributions of the empty cell. The background spectrum of the D2-buffer was subtracted from each sample spectrum on the basis of scaling factors calculated from neutron scattering cross-sections, as reported previously^{35,36}. The temperature was controlled by an LS350 (Lakeshore) with He conductance gas through a GM refrigerator and heat transfer from a cartridge heater installed in a copper block at the top of a sample cell, while monitoring the temperature at the bottom of the cell.

Estimation of the Q10 values. Datasets with more than two temperature points were subjected to Arrhenius plot analysis, and the resulted activation energy (E_a) was converted to the Q10 value at 303 K using $\exp\{(E_a/R)(10/T)/(T+10)\}$, where T and R represent temperature and the gas constant, respectively⁶⁵. Other Q10 values were presented as the ratio of measurement results (R_1 and R_2) at two temperatures (T_1 and T_2) using $Q10 = (R_2/R_1)^{10/(T_2-T_1)}$.

Calculation of D_{global} . The D_{global} values of KaiC^{WT} were simulated at 302 and 313 K using a previously reported method³⁹, the crystal structure (2GBL)³², and HYDROPRO⁶⁶ (Supplementary Note 2).

Reporting summary. Further information on research design is available in the Nature Research Reporting Summary linked to this article.

Data availability

The data that support the findings of this study are available from the corresponding authors upon reasonable request.

Received: 1 September 2021; Accepted: 8 March 2022;

Published online: 04 April 2022

References

- Pittendrigh, C. S. Temporal organization: reflections of a Darwinian clock-watcher. *Annu. Rev. Physiol.* **55**, 16–54 (1993).
- Akiyama, S. Structural and dynamic aspects of protein clocks: how can they be so slow and stable? *Cell. Mol. Life Sci.* **69**, 2147–2160 (2012).
- Ode, K. L. & Ueda, H. R. Design principles of phosphorylation-dependent timekeeping in eukaryotic circadian clock. *Csh. Perspect. Biol.* **10**, a028357 (2018).
- Partch, C. L. Orchestration of circadian timing by macromolecular protein assemblies. *J. Mol. Biol.* **432**, 3426–3448 (2020).
- Narasimamurthy, R. & Virshup, D. M. The phosphorylation switch that regulates ticking of the circadian clock. *Mol. Cell* **81**, 1133–1146 (2021).
- Segel, I. H. *Enzyme Kinetics: Behavior and Analysis of Rapid Equilibrium and Steady State Enzyme Systems* (Wiley, 1975).
- Blandamer, M. J. & Morris, S. H. Investigation into effect of temperature and added tert-butyl alcohol on dynamic properties of Belousov reaction. *J. Chem. Soc. Farad. T.* **1** **71**, 2319–2330 (1975).
- Koros, E. Monomolecular treatment of chemical oscillation. *Nature* **251**, 703–704 (1974).
- Ruoff, P. Antagonistic balance in the oregonator—about the possibility of temperature-compensation in the Belousov-Zhabotinsky reaction. *Phys. D.* **84**, 204–211 (1995).
- Yoshikawa, K. Distinct activation-energies for temporal and spatial oscillations in the Belousov-Zhabotinskii reaction. *B. Chem. Soc. Jpn* **55**, 2042–2045 (1982).
- Mukaiyama, A., Ouyang, D. Y., Furuie, Y. & Akiyama, S. KaiC from a cyanobacterium *Gloeocapsa* sp. PCC 7428 retains functional and structural properties required as the core of circadian clock system. *Int. J. Biol. Macromol.* **131**, 67–73 (2019).
- Terauchi, K. et al. ATPase activity of KaiC determines the basic timing for circadian clock of cyanobacteria. *Proc. Natl Acad. Sci. USA* **104**, 16377–16381 (2007).
- Ito-Miwa, K., Furuie, Y., Akiyama, S. & Kondo, T. Tuning the circadian period of cyanobacteria up to 6.6 days by the single amino acid substitutions in KaiC. *Proc. Natl Acad. Sci. USA* **117**, 20926–20931 (2020).
- Tomita, J., Nakajima, M., Kondo, T. & Iwasaki, H. No transcription-translation feedback in circadian rhythm of KaiC phosphorylation. *Science* **307**, 251–254 (2005).
- Murayama, Y. et al. Tracking and visualizing the circadian ticking of the cyanobacterial clock protein KaiC in solution. *EMBO J.* **30**, 68–78 (2011).
- Isojima, Y. et al. CKI epsilon/delta-dependent phosphorylation is a temperature-insensitive, period-determining process in the mammalian circadian clock. *Proc. Natl Acad. Sci. USA* **106**, 15744–15749 (2009).
- Abe, J. et al. Atomic-scale origins of slowness in the cyanobacterial circadian clock. *Science* **349**, 312–316 (2015).
- Shinohara, Y. et al. Temperature-sensitive substrate and product binding underlie temperature-compensated phosphorylation in the clock. *Mol. Cell* **67**, 783–798 (2017).
- Ruoff, P., Rensing, L., Kommedal, R. & Mohsenzadeh, S. Modeling temperature compensation in chemical and biological oscillators. *Chronobiol. Int.* **14**, 499–510 (1997).
- Hatakeyama, T. S. & Kaneko, K. Generic temperature compensation of biological clocks by autonomous regulation of catalyst concentration. *Proc. Natl Acad. Sci. USA* **109**, 8109–8114 (2012).
- Kurosawa, G. & Iwasa, Y. Temperature compensation in circadian clock models. *J. Theor. Biol.* **233**, 453–468 (2005).
- Das, S., Terada, T. P. & Sasai, M. Single-molecular and ensemble-level oscillations of cyanobacterial circadian clock. *Biophys. Physicobiol.* **15**, 136–150 (2018).
- Sasai, M. Effects of stochastic single-molecule reactions on coherent ensemble oscillations in the KaiABC circadian clock. *J. Phys. Chem. B* **123**, 702–713 (2019).
- Ishiura, M. et al. Expression of a gene cluster *kaiABC* as a circadian feedback process in cyanobacteria. *Science* **281**, 1519–1523 (1998).
- Nakajima, M. et al. Reconstitution of circadian oscillation of cyanobacterial KaiC phosphorylation in vitro. *Science* **308**, 414–415 (2005).
- Nishiwaki, T. et al. A sequential program of dual phosphorylation of KaiC as a basis for circadian rhythm in cyanobacteria. *EMBO J.* **26**, 4029–4037 (2007).

27. Rust, M. J., Markson, J. S., Lane, W. S., Fisher, D. S. & O'Shea, E. K. Ordered phosphorylation governs oscillation of a three-protein circadian clock. *Science* **318**, 809–812 (2007).
28. Bée, M. *Quasielastic Neutron Scattering* (Adam Hilger, 1988).
29. Grimaldo, M., Roosen-Runge, F., Zhang, F., Schreiber, F. & Seydel, T. Dynamics of proteins in solution. *Q. Rev. Biophys.* **52**, 1–63.e7 (2019).
30. Shibata, K. et al. The performance of TOF near backscattering spectrometer DNA in MLF, J-PARC. *JPS Conf. Proc.* **2015** **8**, 036022 (2015).
31. Ouyang, D. Y. et al. Development and optimization of expression, purification, and ATPase assay of KaiC for medium-throughput screening of circadian clock mutants in cyanobacteria. *Int. J. Mol. Sci.* **20**, 2789 (2019).
32. Pattanayek, R. et al. Analysis of KaiA-KaiC protein interactions in the cyanobacterial circadian clock using hybrid structural methods. *EMBO J.* **25**, 2017–2028 (2006).
33. Furuike, Y. et al. Elucidation of master allostery essential for circadian clock oscillation in cyanobacteria. *bioRxiv Preprint at <https://doi.org/10.1101/2021.08.30.457330>* (2021).
34. Murayama, Y. et al. Low temperature nullifies the circadian clock in cyanobacteria through Hopf bifurcation. *Proc. Natl Acad. Sci. USA* **114**, 5641–5646 (2017).
35. Fujiwara, S. et al. Ligation-dependent picosecond dynamics in human hemoglobin as revealed by quasielastic neutron scattering. *J. Phys. Chem. B* **121**, 8069–8077 (2017).
36. Fujiwara, S. et al. Dynamical behavior of human alpha-synuclein studied by quasielastic neutron scattering. *PLoS ONE* **11**, e0151447 (2016).
37. Gibrat, G., Assairi, F. L., Blouquit, Y., Craescu, C. T. & Bellissent-Funel, M. C. Biophysical study of thermal denaturation of apo-calmodulin: dynamics of native and unfolded states. *Biophys. J.* **95**, 5247–5256 (2008).
38. Dee, D. R., Myers, B. & Yada, R. Y. Dynamics of thermodynamically stable, kinetically trapped, and inhibitor-bound states of pepsin. *Biophys. J.* **101**, 1699–1709 (2011).
39. Pérez, J., Zanotti, J. M. & Durand, D. Evolution of the internal dynamics of two globular proteins from dry powder to solution. *Biophys. J.* **77**, 454–469 (1999).
40. Stadler, A. M. et al. Picosecond dynamics in haemoglobin from different species: a quasielastic neutron scattering study. *Biochim. Biophys. Acta* **1840**, 2989–2999 (2014).
41. Zaccai, G. et al. The fluctuating ribosome: thermal molecular dynamics characterized by neutron scattering. *Sci. Rep.* **6**, 37138 (2016).
42. Gaspar, A. M., Appavou, M. S., Busch, S., Unruh, T. & Doster, W. Dynamics of well-folded and natively disordered proteins in solution: a time-of-flight neutron scattering study. *Eur. Biophys. J. Biophys.* **37**, 573–582 (2008).
43. Grimaldo, M., Roosen-Runge, F., Zhang, F. J., Seydel, T. & Schreiber, F. Diffusion and dynamics of gamma-globulin in crowded aqueous solutions. *J. Phys. Chem. B* **118**, 7203–7209 (2014).
44. Matsuo, T., Tominaga, T., Kono, F., Shibata, K. & Fujiwara, S. Modulation of the picosecond dynamics of troponin by the cardiomyopathy-causing mutation K247R of troponin T observed by quasielastic neutron scattering. *BBA-Proteins Proteom.* **1865**, 1781–1789 (2017).
45. Caronna, C., Natali, F. & Cupane, A. Incoherent elastic and quasi-elastic neutron scattering investigation of hemoglobin dynamics. *Biophys. Chem.* **116**, 219–225 (2005).
46. Shrestha, U. R. et al. Effects of pressure on the dynamics of an oligomeric protein from deep-sea hyperthermophile. *Proc. Natl Acad. Sci. USA* **112**, 13886–13891 (2015).
47. Marion, J. et al. Pressure-induced molten globule state of human acetylcholinesterase: structural and dynamical changes monitored by neutron scattering. *Phys. Chem. Chem. Phys.* **17**, 3157–3163 (2015).
48. Golub, M. et al. High hydrostatic pressure specifically affects molecular dynamics and shape of low-density lipoprotein particles. *Sci. Rep.* **7**, 46034 (2017).
49. Fujiwara, S., Matsuo, T., Sugimoto, Y. & Shibata, K. Segmental motions of proteins under non-native states evaluated using quasielastic neutron scattering. *J. Phys. Chem. Lett.* **10**, 7505–7509 (2019).
50. Kataoka, M. et al. Dynamical and structural modifications of staphylococcal nuclease on C-terminal truncation. *Phys. B* **266**, 20–26 (1999).
51. Kataoka, M. et al. Low energy dynamics of globular proteins studied by inelastic neutron scattering. *J. Phys. Chem. Solids* **60**, 1285–1289 (1999).
52. Bu, Z. M. et al. A view of dynamics changes in the molten globule-native folding step by quasielastic neutron scattering. *J. Mol. Biol.* **301**, 525–536 (2000).
53. Grimaldo, M. et al. Hierarchical molecular dynamics of bovine serum albumin in concentrated aqueous solution below and above thermal denaturation. *Phys. Chem. Chem. Phys.* **17**, 4645–4655 (2015).
54. Fujiwara, S., Plazenet, M., Matsumoto, F. & Oda, T. Internal motions of actin characterized by quasielastic neutron scattering. *Eur. Biophys. J. Biophys.* **40**, 661–671 (2011).
55. Chang, Y. G., Tseng, R., Kuo, N. W. & LiWang, A. Rhythmic ring-ring stacking drives the circadian oscillator clockwise. *Proc. Natl Acad. Sci. USA* **109**, 16847–16851 (2012).
56. Philpott, J. M. et al. Casein kinase 1 dynamics underlie substrate selectivity and the PER2 circadian phosphoswitch. *eLife* **9**, e52343 (2020).
57. Fribourgh, J. L. et al. Dynamics at the serine loop underlie differential affinity of cryptochromes for CLOCK:BMAL1 to control circadian timing. *eLife* **9**, e55275 (2020).
58. Hong, L., Vani, B. P., Thiede, E. H., Rust, M. J. & Dinner, A. R. Molecular dynamics simulations of nucleotide release from the circadian clock protein KaiC reveal atomic-resolution functional insights. *Proc. Natl Acad. Sci. USA* **115**, E11475–E11484 (2018).
59. Eisenmesser, E. Z. et al. Intrinsic dynamics of an enzyme underlies catalysis. *Nature* **438**, 117–121 (2005).
60. Terazima, M. Enhanced conformational fluctuations during protein reactions. *Chem. Lett.* **48**, 802–810 (2019).
61. Agarwal, P. K. Role of protein dynamics in reaction rate enhancement by enzymes. *J. Am. Chem. Soc.* **127**, 15248–15256 (2005).
62. Henzler-Wildman, K. A. et al. A hierarchy of timescales in protein dynamics is linked to enzyme catalysis. *Nature* **450**, 913–916 (2007).
63. Hawkins, R. J. & McLeish, T. C. B. Coupling of global and local vibrational modes in dynamic allostery of proteins. *Biophys. J.* **91**, 2055–2062 (2006).
64. Agarwal, P. K. A biophysical perspective on enzyme catalysis. *Biochemistry* **58**, 438–449 (2019).
65. Furuike, Y., Abe, J., Mukaiyama, A. & Akiyama, S. Accelerating in vitro studies on circadian clock systems using an automated sampling device. *Biophys. Physicobiol.* **13**, 235–241 (2016).
66. Ortega, A., Amoros, D. & de la Torre, J. G. Prediction of hydrodynamic and other solution properties of rigid proteins from atomic- and residue-level models. *Biophys. J.* **101**, 892–898 (2011).

Acknowledgements

We thank Dr. K. Shibata for his kind support for the trial QENS experiment, and Dr. M. Kataoka and Dr. H. Kamikubo for their discussions and critical comments on the manuscript. This study was partly supported by Grants-in-Aid for Scientific Research (17H06165 to S.A.). The QENS experiments using BL02 (DNA) at the Materials and Life Science Experimental Facility of the J-PARC were performed under user programs (Proposal No. 2017B0123, 2018B0244, 2019A0308, and 2020B0073).

Author contributions

Y.F. and S.A. designed the study; Y.F., D.O., T.M., and A.M. prepared samples; Y.F. and D.O. conducted biochemical assays; Y.F., T.T., T.M., Y.K., S.F., and S.A. performed QENS experiments; Y.F., T.T., T.M., Y.K., S.F., and S.A. analyzed QENS data; and S.A., S.F., and Y.F. wrote the paper with input from all authors.

Competing interests

The authors declare no competing interests.

Additional information

Supplementary information The online version contains supplementary material available at <https://doi.org/10.1038/s42005-022-00852-z>.

Correspondence and requests for materials should be addressed to Satoru Fujiwara or Shuji Akiyama.

Peer review information *Communications Physics* thanks Andreas Stadler, Yong-Ick Kim and the other, anonymous, reviewer(s) for their contribution to the peer review of this work.

Reprints and permission information is available at <http://www.nature.com/reprints>

Publisher's note Springer Nature remains neutral with regard to jurisdictional claims in published maps and institutional affiliations.



Open Access This article is licensed under a Creative Commons Attribution 4.0 International License, which permits use, sharing, adaptation, distribution and reproduction in any medium or format, as long as you give appropriate credit to the original author(s) and the source, provide a link to the Creative Commons license, and indicate if changes were made. The images or other third party material in this article are included in the article's Creative Commons license, unless indicated otherwise in a credit line to the material. If material is not included in the article's Creative Commons license and your intended use is not permitted by statutory regulation or exceeds the permitted use, you will need to obtain permission directly from the copyright holder. To view a copy of this license, visit <http://creativecommons.org/licenses/by/4.0/>.

© The Author(s) 2022